Energy & Environmental Science

Cite this: *Energy Environ. Sci.*, 2012, **5**, 6098

www.rsc.org/ees

PAPER

Syngas production by simultaneous splitting of H_2O and CO_2 *via* ceria redox reactions in a high-temperature solar reactor

Philipp Furler,[a] Jonathan R. Scheffe[a] and Aldo Steinfeld*[ab]

Received 8th September 2011, Accepted 24th October 2011
DOI: 10.1039/c1ee02620h

Solar syngas production from H_2O and CO_2 is experimentally investigated using a two-step thermochemical cycle based on cerium oxide redox reactions. A solar cavity-receiver containing porous ceria felt is directly exposed to concentrated thermal radiation at a mean solar concentration ratio of 2865 suns. In the first endothermic step at 1800 K, ceria is thermally reduced to an oxygen deficient state. In the second exothermic step at 1100 K, syngas is produced by re-oxidizing ceria with a gas mixture of H_2O and CO_2. The syngas composition is experimentally determined as a function of the molar co-feeding ratio H_2O : CO_2 in the range of 0.8 to 7.7, yielding syngas with H_2 : CO molar ratios from 0.25 to 2.34. Ten consecutive H_2O/CO_2-splitting cycles performed over an 8 hour solar experimental run are presented.

1. Introduction

Syngas, the precursor to liquid hydrocarbon fuels, can be produced from CO_2 and H_2O by a 2-step thermochemical cycle using a variety of metal oxide redox materials.[1,2] In contrast to the direct thermolysis, these cycles bypass the CO/O_2 and H_2/O_2 separation problem and operate at lower temperatures. However, ZnO, SnO_2, and analogous volatile oxides that sublime during decomposition require rapid quenching of gaseous products to avoid recombination,[3,4] while non-volatile oxides such as ferrite-based oxides suffer from relatively slow kinetics, sintering, and material losses due to undesired volatilization.[5–11] Non-stoichiometric cerium oxide has emerged as an attractive redox active material because of its relatively high oxygen ion conductivity and cyclability when its fluorite-type structure and phase are maintained.[12–17] The two-step H_2O/CO_2 splitting solar thermochemical cycle based on oxygen-deficient ceria is represented by:

$$\text{High-T reduction}: \quad CeO_2 \xrightarrow{\Delta H} CeO_{2-\delta} + \frac{\delta}{2}O_2 \qquad (1)$$

$$\text{Low-T oxidation with } H_2O: CeO_{2-\delta} + \delta H_2O \rightarrow CeO_2 + \delta H_2 \qquad (2)$$

$$\text{Low-T oxidation with } CO_2: CeO_{2-\delta} + \delta CO_2 \rightarrow CeO_2 + \delta CO \qquad (3)$$

In the first high-temperature step, the ceria is thermally reduced to a non-stoichiometric state (T > 1673 K). In the proceeding, lower temperature steps, ceria is re-oxidized with H_2O and/or CO_2 to produce H_2 and/or CO, respectively (T < 1673 K).[18,19] We have recently demonstrated, in separate experimental solar runs, the production of H_2 from H_2O and of CO from CO_2 using a solar cavity-receiver containing porous monolithic ceria.[20] In this work, we use the same geometrical cavity-type configuration, this time packed with porous ceria felt, to co-produce H_2 and CO (syngas) by simultaneously splitting a mixture of H_2O and CO_2. The co-feeding molar ratio H_2O : CO_2 is varied to examine its influence on the H_2 : CO molar ratio. Consecutive splitting cycles are performed to assess cyclability. No attempt was undertaken

[a]*Department of Mechanical and Process Engineering, ETH Zurich, 8092 Zurich, Switzerland. E-mail: aldo.steinfeld@ethz.ch*
[b]*Solar Technology Laboratory, Paul Scherrer Institute, 5232 Villigen PSI, Switzerland*

Broader context

Syngas—the precursor to synthetic liquid hydrocarbon fuels—is produced from H_2O and CO_2 *via* a two-step solar thermochemical cycle with ceria redox reactions. Concentrated solar energy is used as the source of high-temperature process heat to drive the endothermic reactions. The cyclic process is experimentally demonstrated with a 3 kW solar cavity receiver-reactor containing porous ceria felt and directly exposed to high-flux (>2800 suns) thermal radiation. The H_2 : CO molar ratios of the syngas are controlled by adjusting the H_2O : CO_2 molar ratio. Ten consecutive H_2O/CO_2-splitting cycles are performed over 8 hours, yielding a constant and stable syngas composition.

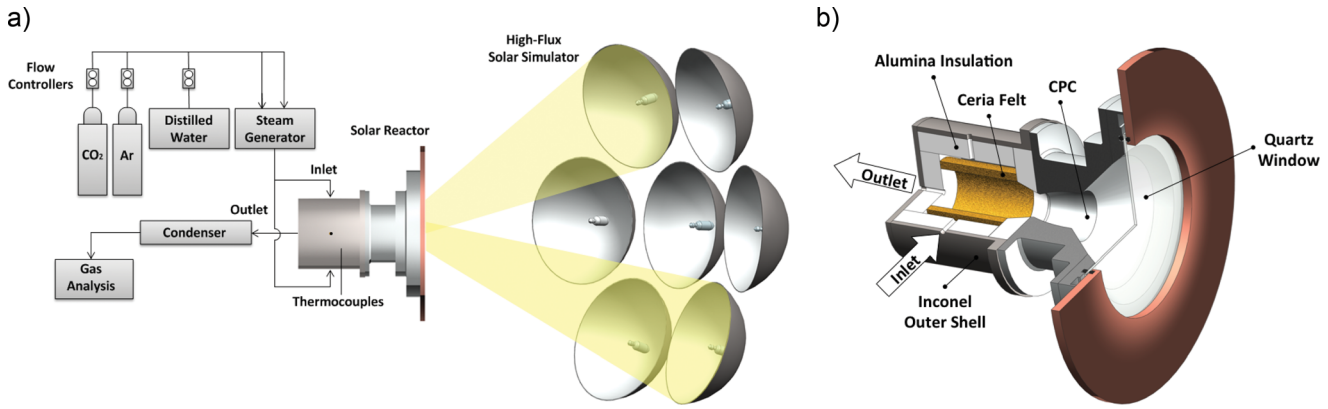

Fig. 1 (a) Experimental setup of ETH's High-Flux Solar Simulator and (b) schematic of the solar reactor configuration.

to optimize the solar reactor for maximum solar-to-fuel energy conversion efficiency.

2. Experimental setup and methods

The experimental setup is shown schematically in Fig. 1a; the solar reactor configuration is depicted in Fig. 1b. Experimentation was performed at the High-Flux Solar Simulator (HFSS) of ETH Zurich. An array of seven Xe arcs, close-coupled to truncated ellipsoidal reflectors, provided an external source of intense thermal radiation (mostly in the visible and IR spectra) that closely approximated the heat transfer characteristics of highly concentrating solar systems, such as solar towers and dishes.[21] The solar reactor consisted of a cavity-receiver with a 4 cm dia. circular aperture for the access of concentrated solar radiation. The aperture was closed by a 24 cm dia., 3 mm thick clear fused quartz disk window. A compound parabolic concentrator (CPC) was incorporated into the aperture to further boost the solar concentration ratio† to mean values of 2865 suns. The cavity contained a 62 mm i.d., 85 mm o.d., 100 mm height cylinder made of various layers of porous ceria felt (Zircar Zirconia, Type CeF-100, 99+% purity, 96% bulk porosity, 127 g in mass). With this arrangement, the inner walls of the ceria felt cylinder were directly exposed to the high-flux irradiation. The cavity was lined by Al_2O_3-insulation (Zircar Zirconia, Type BusterM-35) and sheathed by the outer shell made of Inconel 600. Temperatures were measured in the middle of the ceria felt (B-type thermocouples; 5 mm radial distance from inner ceria layer, 50 mm from bottom plate); in the center of the Al_2O_3-insulation at different heights (K-type thermocouples, 13, 50, and 90 mm from bottom plate), and in the Inconel wall (K-type thermocouples, side wall and bottom plate). An annular gap between the ceria felt and the Al_2O_3-insulation prevented undesired side reactions and enabled uniform cross-flow. Purge gas (Ar 5.0, O_2 < 2 ppm) and CO_2 flow rates (4.8, O_2 < 2 ppm) were regulated by electronic mass flow controllers (Bronkhorst F-201C). H_2O at 473 K was delivered by a steam generator (Bronkhorst W-303-120-P) that was regulated by a liquid mass flow controller (Bronkhorst L2-FAC-11-0). All inlet gases were introduced through four radial inlet ports. Product gases exited the reactor through an outlet port at the center of the bottom plate. Product gas composition was monitored by gas chromatography (Varian 490), supplemented by a paramagnetic alternating pressure based O_2 detector (Siemens Oxymat 6), infrared-based detectors for CO and CO_2 (Siemens Ultramat 23), and a thermal conductivity-based detector for H_2 (Siemens Calomat 6). The radiative flux distribution at the focal plane of the solar concentrator was measured optically prior to each experimental run using a calibrated CCD camera focused on a water-cooled, Al_2O_3-plasma-coated Lambertian (diffusely reflecting) target. The radiative power input through the aperture Q_{solar} was measured using a water-calorimeter.

Single H_2O/CO_2 co-feeding cycles—Prior to starting a run, the reactor was heated for 10 min at a radiative power input of 0.8 kW and purged with an Ar flow rate of 2 l min^{-1} (SLPM, mass flow rates calculated at 273.15 K and 101 325 Pa). The Ar flow was kept constant at a rate of 2 l min^{-1} during both reduction and oxidation steps. Thermal reduction was performed using 3.6 kW radiative power input with a mean solar concentration ratio of 2865 suns over the aperture. Thermal reduction was terminated when the rate of O_2-release dropped to 20% of its peak value. This was accomplished by turning off the HFSS for 4.5 minutes, followed by an increase of the radiative power input to 0.8 kW to stabilize temperatures and approach steady-state operation. Oxidation was initiated by injecting a mixture of steam and CO_2 with a total flow rate of 2.5 l min^{-1}. After 15 minutes, the reactant gas flow was turned off and purged from the reactor. The following H_2O : CO_2 molar ratios were investigated: 0.8, 2.6, 4, 5.7, 7.7, with three random replicates each for reproducibility.

Consecutive H_2O/CO_2 co-feeding cycles—The Ar flow was kept constant at a rate of 2 l min^{-1} during both reduction and oxidation steps. Each thermal reduction step was performed using 3.6 kW radiative power input during a 30 min time interval and terminated by reducing the radiative power input to 0.7 kW. Immediately afterwards, a mixture of H_2O and CO_2 with a H_2O : CO_2 molar ratio of 6.7 was injected at a total mass flow rate of 2.53 l min^{-1}. Oxidation was performed during a 15 min time interval and terminated by turning off the flow of reactants. Thermal reduction of the next cycle was reinitiated by resuming the radiative power input to 3.6 kW.

† The solar concentration ratio C is defined as $C = Q_{solar}/(IA)$, where Q_{solar} is the solar radiative power intercepted by the aperture of area A. C is often expressed in units of "suns" when normalized to $I = 1$ kW m^{-2}.

Sample morphology and composition were analyzed *via* scanning electron microscopy and energy dispersive X-ray spectroscopy (Hitachi TM-1000).

3. Results and discussion

Fig. 2 shows the variation of the temperature of the ceria felt and the O_2/syngas evolution rate during a representative single cycle experiment performed at a $H_2O : CO_2$ molar ratio of 5.7. A rapid temperature increase of the ceria (400 K min^{-1} below 1600 K, afterwards 20 K min^{-1}, averaged rate of 65 K min^{-1}) was observed shortly after increasing the radiative power input from 0.8 kW to 3.6 kW, leading to temperatures in the range 1733–1920 K, depending on the location. Above 1200 K, O_2 evolution was observed and reached maximum and average rates of 0.21 ± 0.02 ml min^{-1} g^{-1} CeO_2 and 0.11 ± 0.01 ml min^{-1} g^{-1} CeO_2, respectively. Total O_2 evolution was 2.89 ± 0.27 ml g^{-1} CeO_2, corresponding to a $\delta = 0.044 \pm 0.004$. This is slightly lower than 4.3 ± 0.3 ml g^{-1} CeO_2 or $\delta = 0.066 \pm 0.005$ determined in a small scale infrared furnace[15] but comparable to values between 3 ml g^{-1} CeO_2 and 4 ml g^{-1} CeO_2 measured by thermogravimetry.[17,22] After termination of the first reaction step, the temperature of the ceria decreased rapidly to 1200 K within 4.5 min. Shortly after injecting the H_2O/CO_2 mixture, rapid production of H_2 and CO was observed with peak reaction rates of 1.923 ± 0.47 ml min^{-1} g^{-1} CeO_2, average fuel production rates of 0.39 ± 0.03 ml min^{-1} g^{-1} CeO_2, and a total fuel production of 5.88 ± 0.43 ml g^{-1} CeO_2. A reactant gas utilization of 9.5% (CO_2: 22.4%, H_2O: 7.1%) was observed at peak syngas production rates. Syngas containing unreacted CO_2 in concentrations such as those occurring at the outlet of our reactor can be processed to liquid hydrocarbon fuels *via* Fischer–Tropsch, depending on the desired liquid product, operating temperature, pressure, and catalyst.[23] Otherwise, if CO_2 needs to be removed, a variety of commercially viable technologies are available such as physical/chemical absorption, pressure/temperature swing adsorption, membrane technology, and cryogenic CO_2 separation.[24] The ratio of fuel produced to oxygen released was 2.04 ± 0.05, implying that the oxygen nonstoichiometry was fully used for fuel production. During experimentation, no gas-phase hydrocarbons were detected by GC and no deposition of carbon on the ceria or insulation was observed, indicating that total selectivity toward syngas production was achieved.

Fig. 3 shows the $H_2 : CO$ molar ratio of the syngas produced as a function of the $H_2O : CO_2$ molar ratio of the reacting gas mixture. The $H_2 : CO$ molar ratio increased linearly from 0.25 to 2.34 for $H_2O : CO_2$ molar ratios varying from 0.8 to 7.7. According to these results, co-feeding with $H_2O : CO_2 = 5.6$ yields syngas with $H_2 : CO = 1.7$, which is suitable for the processing of liquid fuels (*e.g.* diesel, kerosene) *via* low-temperature Fischer–Tropsch.[25,26] Syngas with $H_2 : CO = 2$ was obtained by reacting 15% Sm-doped ceria with $H_2O : CO_2 = 2$ in a packed bed at 1173 K.[14] Syngas with $H_2 : CO$ molar ratios that corresponded to the $H_2O : CO_2$ molar ratios in the inlet flow was obtained by reacting Zn particles with shortage of H_2O and CO_2 in a packed-bed at 680 K.[27]

Fig. 4 shows the equilibrium $H_2 : CO$ molar ratio as a function of the $H_2O : CO_2$ molar ratio of the reacting gas mixture for various temperatures in the range 800–1800 K, calculated with HSC software.[28] Experimentally measured $H_2 : CO$ molar ratios are additionally indicated. $H_2 : CO$ ratios decrease with temperature as CO_2 reduction becomes thermodynamically favorable compared to H_2O reduction, and can be explained in part by the reverse water–gas shift reaction. The equilibrium values match our experimentally determined ones at 1650 K, indicating that during oxidation higher temperatures were presumably reached at the directly irradiated innermost ceria layer than those measured by the inserted thermocouples (~1100 K).

Fig. 5 shows ten consecutive H_2O/CO_2 splitting cycles performed over 8 hours at a constant feeding ratio ($H_2O : CO_2 = 6.7$), yielding syngas with an average $H_2 : CO$ ratio of 2.36 ± 0.07. Consistent with single cycle experiments, production of

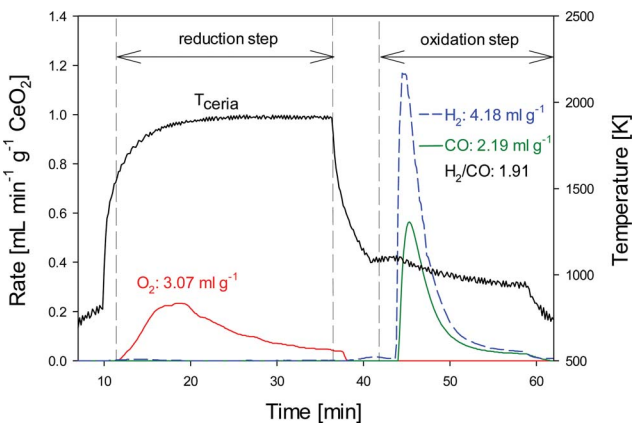

Fig. 2 Temperature of the ceria felt, O_2 and syngas evolution rate during a two-step redox ceria cycle. *Experimental conditions*: 3.6 and 0.8 kW radiative power input during reduction and oxidation steps, respectively; 2 l min^{-1} Ar purge gas during both reduction and oxidation steps; 2.15 l min^{-1} H_2O and 0.375 l min^{-1} CO_2 during the oxidation step for a $H_2O : CO_2$ molar ratio of 5.7.

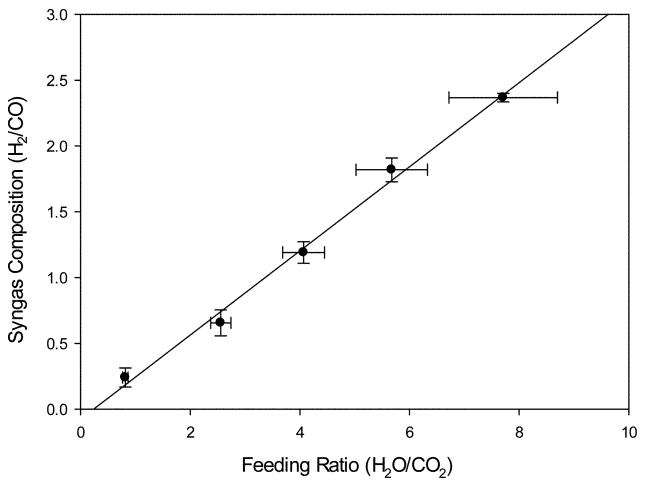

Fig. 3 $H_2 : CO$ molar ratio of the syngas produced as a function of the $H_2O : CO_2$ molar ratio of the reacting gas mixture. Error bars in *x*-direction indicate the error of the flow controllers, error bars in *y*-direction indicate the standard deviation from the experimentally measured and averaged composition.

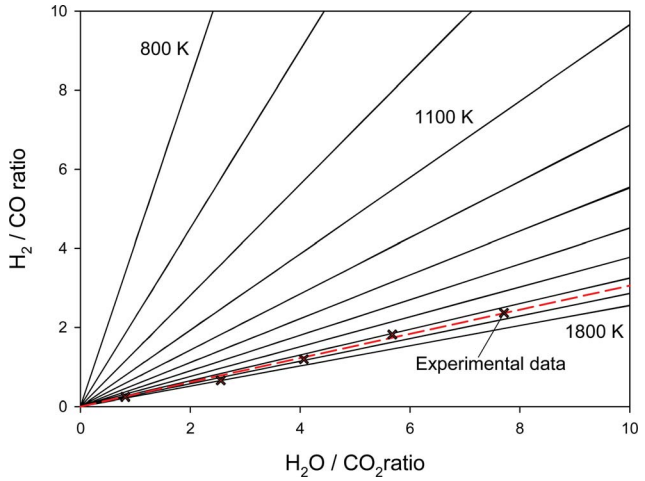

Fig. 4 Thermodynamic equilibrium H_2 : CO molar ratio as a function of the H_2O : CO_2 molar ratio of the reacting gas mixture for various temperatures in the range 800–1800 K. Experimentally measured H_2 : CO molar ratios are indicated.

syngas was immediately observed after injection of the H_2O/CO_2 mixture, reaching an average peak rate of 0.48 ± 0.08 ml min^{-1} g^{-1} CeO_2 (H_2: 0.32 ± 0.06 ml min^{-1} g^{-1} CeO_2, CO: 0.16 ± 0.03 ml min^{-1} g^{-1} CeO_2), an average rate of 0.2 ± 0.01 ml min^{-1} g^{-1} CeO_2 (H_2: 0.14 ± 0.03 ml min^{-1} g^{-1} CeO_2, CO: 0.06 ± 0.01 ml min^{-1} g^{-1} CeO_2), and a total fuel production of 3.15 ± 0.49 ml g^{-1} CeO_2 (H_2: 2.21 ± 0.34 ml g^{-1} CeO_2, CO: 0.94 ± 0.15 ml g^{-1} CeO_2). The average peak rate and average rate of O_2 evolution were 0.08 ± 0.02 ml min^{-1} g^{-1} CeO_2 and 0.05 ± 0.01 ml min^{-1} g^{-1} CeO_2, respectively, and the total O_2 release was 1.52 ± 0.27 ml g^{-1} CeO_2 ($\delta = 0.023 \pm 0.004$). A slight decline in peak reactor temperature, from 1855 K to 1767 K, which was attained during the reduction steps, caused a gradual reduction in O_2 release and fuel yield. An opaque thin film deposited on the compound parabolic concentrator (CPC) was identified as CeO_2 by EDS analysis. This film likely reduced the CPC reflectivity and resulted in less radiative power input through the aperture, explaining the slight decrease in temperature. Presumably, ceria sublimated during reduction and condensed at the water-cooled walls of the CPC surface. Ceria sublimation at above 1673 K has been observed previously.[17,22] It could potentially be avoided by applying vacuum pressure to shift the equilibrium to lower reduction temperatures and prevent back diffusion of CeO_2 gas. It is likely that higher temperatures were achieved on the innermost surface than those measured by the thermocouples due to the insulating nature of the felt. SEM micrographs shown in Fig. 6 support this hypothesis, and indicate that more sintering was observed on the innermost surface compared to the outer layer.

The average and peak instantaneous solar-to-fuel energy conversion efficiencies are defined as:

$$\eta_{\text{average}} = \frac{\Delta H_{\text{fuel}} \int r_{\text{fuel}} \mathrm{d}t}{\int P_{\text{solar}} \mathrm{d}t + E_{\text{inert}} \int r_{\text{inert}} \mathrm{d}t}$$

$$\eta_{\text{peak}} = \frac{2 r_{\text{oxygen}} \Delta H_{\text{fuel}}}{P_{\text{solar}} + r_{\text{inert}} E_{\text{inert}}}$$

where r_{fuel} is the molar fuel production rate, r_{oxygen} is the molar O_2 release rate during reduction, ΔH_{fuel} is the high heating value of the fuel, P_{solar} is the radiative power input, r_{inert} is the flow rate of the inert gas during reduction, and E_{inert} is the energy required to separate the inert sweep gas from air (20 kJ mol^{-1}).[29] η_{average} is calculated by integration over the time required to produce 80% of the fuel, but accounting for P_{solar} during both oxidation and reduction steps. η_{peak} is calculated based on the peak O_2 release rate achieved during reduction whereby a stoichiometric fuel production and no energy input during the exothermic oxidation

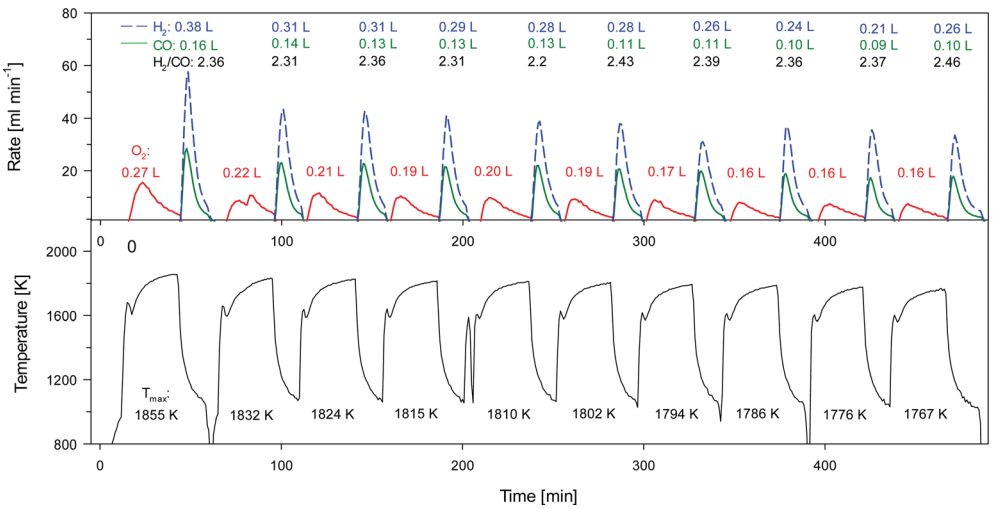

Fig. 5 Temperature of the ceria felt, gas production rates, total amount of evolved gases, and H_2 : CO molar ratios during ten consecutive splitting cycles. *Experimental conditions*: 3.6 and 0.7 kW radiation power input during reduction and oxidation steps, respectively; 2 l min^{-1} Ar purge gas during both reduction and oxidation steps; 2.2 l min^{-1} H_2O and 0.33 l min^{-1} CO_2 during the oxidation step (H_2O : CO_2 molar ratio of 6.7). The reduction and oxidation steps were performed at constant time intervals of 30 and 15 minutes, respectively.

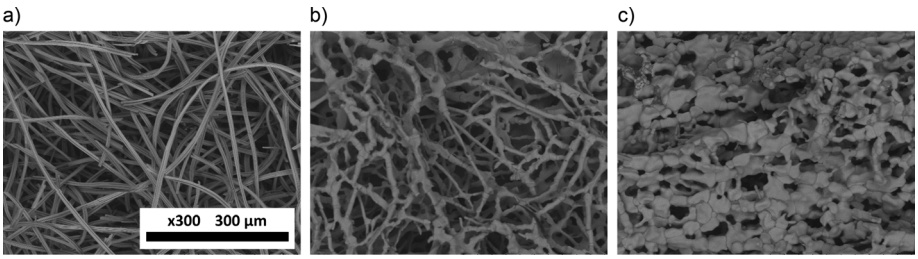

Fig. 6 (a) SEM micrographs of unreacted ceria felt, (b) the outermost surface of the ceria felt, and (c) the innermost ceria felt after the experimental campaign.

are assumed. Based on the experimental data, $\eta_{average} = 0.15\%$ and $\eta_{peak} = 0.31\%$ were obtained for the single H_2O/CO_2-co-feeding cycle, and $\eta_{average} = 0.09\%$ and $\eta_{peak} = 0.16\%$ were obtained for the ten consecutive H_2O/CO_2-co-feeding cycles. Previous work on separate CO_2 and H_2O dissociation performed with porous monolithic bricks (total mass: 325 g) in a similar solar reactor configuration resulted in $\eta_{average} = 0.4\%$ and $\eta_{peak} = 0.8\%$.[20] We attribute the lower efficiencies observed in this study to a lower ceria loading and active material, as reaction took place predominantly at the innermost layer of felt exposed to high-flux radiation. The low thermal conductivity of ceria felt resulted in an undesired temperature gradient across the felt, so that the concentric layers on the outside did not reach the high temperatures achieved on the innermost surface and consequently a gradient in the amount of CeO_2 reduction is assumed. A more homogeneous temperature distribution may be obtained by employing a macroporous ceria structure (*e.g.* reticulate foam) that enables penetration and volumetric absorption of concentrated solar radiation. A thermodynamic analysis based solely on the material properties of CeO_2 indicates that efficiency values in the range of 16–19% are attainable, even in the absence of sensible heat recovery.[15] A recent report has indicated that solar fuels produced with 20% efficiency are likely to be cost competitive.[30] No attempt was undertaken in this study to optimize the solar reactor design/operation for maximum solar-to-fuel energy conversion efficiency.

4. Summary and conclusions

Syngas production by simultaneous splitting of H_2O and CO_2 *via* a thermochemical redox cycle has been demonstrated using a porous ceria felt arranged inside a solar cavity-receiver directly exposed to concentrated thermal radiation. The observed average O_2 release during the reduction step was 2.89 ± 0.27 ml g^{-1} CeO_2 and fuel production during the oxidation step was 5.88 ± 0.43 ml g^{-1} CeO_2. The H_2 : CO molar ratios of the syngas were controlled in a range from 0.25 to 2.34 by adjusting the H_2O : CO_2 molar ratio from 0.8 to 7.7. Sublimation of ceria and deposition on the CPC resulted in a reduced radiative power input through the aperture and consequently lowered temperatures and fuel yield. Ten consecutive H_2O/CO_2 gas splitting cycles have been performed over 8 hours, yielding a constant and stable syngas composition. The results demonstrate the feasibility of ceria-based redox cycles to produce repetitive and controlled amounts of syngas in a solar reactor that closely replicates conditions expected in practical solar fuel applications.

Nomenclature

A	area (m^2)
C	solar concentration ratio
E_{inert}	energy required to separate the inert gas from the air
GC	gas chromatography/chromatograph
ΔH_{fuel}	higher heating value of the fuel (J mol^{-1})
ΔH	reaction enthalpy (J mol^{-1})
I	direct normal solar irradiation (W m^{-1})
P_{solar}	radiation power input (W)
Q_{solar}	solar power input (W)
p	pressure (Pa)
r_{fuel}	molar fuel production rate (mol s^{-1})
r_{oxygen}	molar oxygen release rate (mol s^{-1})
r_{inert}	flow rate of inert gas (mol s^{-1})
T	temperature (K)

Greek letters

δ	ceria nonstoichiometry
$\eta_{average}$	average solar-to-fuel energy conversion efficiency
η_{peak}	peak instantaneous solar-to-fuel energy conversion efficiency

Abbreviations

HFSS	High-Flux Solar Simulator
EDS	energy dispersive spectroscopy
CCD	charge-coupled device
CPC	compound parabolic concentrator
SLPM	standard litres per minute, calculated at 273.15 K and 101 325 Pa

Acknowledgements

This work has been financially supported by the European Commission under contract No. 285098 (Project SOLAR-JET).

We thank P. Haueter and D. Hermann for technical support during the experimental campaign.

References

1 A. Steinfeld, *Sol. Energy*, 2005, **78**, 603–615.
2 C. Perkins and A. W. Weimer, *Int. J. Hydrogen Energy*, 2004, **29**, 1587–1599.
3 P. G. Loutzenhiser, A. Meier and A. Steinfeld, *Materials*, 2010, **3**, 4922–4938.
4 M. Chambon, S. Abanades and G. Flamant, *AIChE J.*, 2011, **57**, 2264–2273.
5 P. Charvin, S. Abanades, G. Flamant and F. Lemort, *Energy*, 2007, **32**, 1124–1133.
6 F. Fresno, R. Fernández-Saavedra, M. Belén Gómez-Mancebo, A. Vidal, M. Sánchez, M. Isabel Rucandio, A. J. Quejido and M. Romero, *Int. J. Hydrogen Energy*, 2009, **34**, 2918–2924.
7 M. Roeb, C. Sattler, R. Kluser, N. Monnerie, L. de Oliveira, A. G. Konstandopoulos, C. Agrafiotis, V. T. Zaspalis, L. Nalbandian, A. Steele and P. Stobbe, *J. Sol. Energy Eng.*, 2006, **128**, 125–133.
8 N. Gokon, H. Murayama, A. Nagasaki and T. Kodama, *Sol. Energy*, 2009, **83**, 527–537.
9 H. Ishihara, H. Kaneko, N. Hasegawa and Y. Tamaura, *Energy*, 2008, **33**, 1788–1793.
10 J. Miller, M. Allendorf, R. Diver, L. Evans, N. Siegel and J. Stuecker, *J. Mater. Sci.*, 2008, **43**, 4714–4728.
11 M. D. Allendorf, R. B. Diver, N. P. Siegel and J. E. Miller, *Energy Fuels*, 2008, **22**, 4115–4124.
12 S. Abanades and G. Flamant, *Sol. Energy*, 2006, **80**, 1611–1623.
13 H. Kaneko, T. Miura, H. Ishihara, S. Taku, T. Yokoyama, H. Nakajima and Y. Tamaura, *Energy*, 2007, **32**, 656–663.
14 W. Chueh and S. Haile, *ChemSusChem*, 2009, **2**, 735–739.
15 W. Chueh and S. Haile, *Philos. Trans. R. Soc. London, Ser. A*, 2010, **368**, 3269–3294.
16 P. Singh and M. S. Hegde, *Chem. Mater.*, 2009, **22**, 762–768.
17 S. Abanades, A. Legal, A. Cordier, G. Peraudeau, G. Flamant and A. Julbe, *J. Mater. Sci.*, 2010, **45**, 4163–4173.
18 M. Zinkevich, D. Djurovic and F. Aldinger, *Solid State Ionics*, 2006, **177**, 989–1001.
19 G. Zhou, P. R. Shah, T. Montini, P. Fornasiero and R. J. Gorte, *Surf. Sci.*, 2007, **601**, 2512–2519.
20 W. C. Chueh, C. Falter, M. Abbott, D. Scipio, P. Furler, S. M. Haile and A. Steinfeld, *Science*, 2010, **330**, 1797–1801.
21 J. Petrasch, P. Coray, A. Meier, M. Brack, P. Haberling, D. Wuillemin and A. Steinfeld, *J. Sol. Energy Eng.*, 2007, **129**, 405–411.
22 R. Panlener, R. Blumenthal and J. Garnier, *J. Phys. Chem. Solids*, 1975, **36**, 1213–1222.
23 T. Riedel and G. Schaub, *Top. Catal.*, 2003, **26**, 145–156.
24 G. Göttlicher and R. Pruschek, *Energy Convers. Manage.*, 1997, **38**(suppl. 1), S173–S178.
25 J. Strege, M. Swanson, B. Folkedahl, J. Stanislowski and J. Laumb, *Fuel Process. Technol.*, 2011, **92**, 757–763.
26 M. E. Dry, *Catal. Today*, 2002, **71**, 227–241.
27 A. Stamatiou, P. G. Loutzenhiser and A. Steinfeld, *AIChE J.*, 2011, DOI: 10.1002/aic.12580.
28 A. Roine, Outokumpu Research Oy, Pori, Finland, 2002.
29 H.-W. Haering, *Industrial Gases Processing*, Wiley-VHC, 2008.
30 J. Kim, C. A. Henao, T. A. Johnson, D. E. Dedrick, J. E. Miller, E. B. Stechel and C. T. Maravelias, *Energy Environ. Sci.*, 2011, **4**, 3122–3132.